

Can a Fast-mode EUV Wave Generate a Stationary Front?

P. F. Chen^{1,2} · C. Fang^{1,2} · R. Chandra³ · A. K. Srivastava⁴

© Springer

Abstract The discovery of stationary “EIT waves” about 16 years ago posed a big challenge to the then favorite fast-mode wave model for coronal “EIT waves”. It encouraged the proposing of various non-wave models, and played an important role in approaching the recent converging viewpoint, *i.e.* there are two types of EUV waves. However, it was recently discovered that a stationary wave front can also be generated when a fast-mode wave passes through a magnetic quasi-separatrix layer (QSL). In this paper, we perform a magnetohydrodynamic (MHD) numerical simulation of the interaction between a fast-mode wave and a magnetic QSL, and a stationary wave front is reproduced. The analysis of the numerical results indicates that near the plasma beta ~ 1 layer in front of the magnetic QSL, part of the fast-mode wave is converted to a slow-mode MHD wave, which is then trapped inside the magnetic loops, forming a stationary wave front. Our research implies that we have to be cautious in identifying the nature of a wave since there may be mode conversion during the propagation of the waves driven by solar eruptions.

Keywords: Magnetohydrodynamics; Corona; Waves; Magnetic fields

1. Introduction

One of the most intriguing phenomena discovered by the *EUV Imaging Telescope* (EIT, Delaboudinière *et al.*, 1995) aboard the Solar and Heliospheric

✉ P. F. Chen
chenpf@nju.edu.cn

¹ School of Astronomy & Space Science, Nanjing University, Nanjing 210023, China

² Key Lab for Modern Astronomy and Astrophysics (Nanjing University), Ministry of Education, Nanjing 210023, China

³ Department of Physics, DSB Campus, Kumaun University, Nainital 263001, India

⁴ Department of Physics, Indian Institute of Technology (BHU), Varanasi 221005, India

Observatory (SOHO) spacecraft is the so-called “EIT waves”, which are named after the observing telescope (Moses *et al.*, 1997; Thompson *et al.*, 1998, 1999). “EIT waves” are bright fronts visible in various EUV wavelengths (Wills-Davey and Thompson, 1999; Long *et al.*, 2008; Kumar *et al.*, 2013), such as 171 Å (formation temperature of 0.63 MK, Wills-Davey and Thompson, 1999), 193 Å (formation temperature 1.2 MK, Thompson *et al.*, 1998), and 211 Å (formation temperature 2 MK, Kumar *et al.*, 2013), and 284 Å (formation temperature 2.25 MK, Zhukov and Auchère, 2004). They commence following coronal mass ejections (CMEs)/flare eruptions. It has been verified that they are more related to CMEs, rather than solar flares (Biesecker *et al.*, 2002; Chen, 2006, 2011).

When “EIT waves” were discovered, they were initially explained to be fast-mode waves (or shock waves) driven by CME/flare eruptions (Thompson *et al.*, 1998; Wang, 2000; Wu *et al.*, 2001; Ofman and Thompson, 2002; Vršnak *et al.*, 2002; Veronig, Temmer, and Vršnak, 2008), and they were thought to be the coronal counterparts of chromospheric Moreton waves (Thompson *et al.*, 1998; Grechnev *et al.*, 2014, 2015). However, the primary drawback of the fast-mode wave model is that the velocities of the “EIT waves” are typically ~ 3 times smaller than those of the coronal fast-mode shock waves that are inferred from type II radio bursts (Klassen *et al.*, 2000) or from chromospheric Moreton waves (Zhang *et al.*, 2011).

More importantly, soon after “EIT waves” were discovered, Delannée and Aulanier (1999) and Delannée (2000) revealed that the wave fronts in several “EIT wave” events are stationary, and the stationary “EIT wave” front was found to be cospatial with a magnetic quasi-separatrix layer (QSL), across which magnetic field lines change connectivity rapidly. Since it is generally thought that fast-mode wave would travel across the magnetic QSL, the discovery of stationary “EIT wave” fronts led Delannée and Aulanier (1999) and Delannée (2000) to doubt the fast-mode wave model for “EIT waves”. They proposed that “EIT waves” are related magnetic reconfiguration.

Encouraged by their questioning on the fast-mode wave model, several other models have been proposed, *e.g.* the magnetic fieldline stretching model (Chen *et al.*, 2002; Chen, Fang, and Shibata, 2005b), successive reconnection model (Attrill *et al.*, 2007a,b; van Driel-Gesztelyi *et al.*, 2008; Cohen *et al.*, 2009, 2010), the slow-mode wave model (Wills-Davey, DeForest, and Stenflo, 2007; Wang, Shen, and Lin, 2009), and the current shell model (Delannée *et al.*, 2008). Taking the magnetic fieldline stretching model for an example, the “EIT waves” discovered by Thompson *et al.* (1998) are believed to be generated by the successive stretching of the closed magnetic field lines pushed by an erupting flux rope below. In particular, with magnetohydrodynamic (MHD) numerical simulations, Chen, Fang, and Shibata (2005b) confirmed that “EIT waves” would stop at magnetic QSLs. The reason is straightforward, *i.e.* on the other side of the magnetic QSL, the magnetic field lines belong to another flux system, which cannot be pushed to stretch up by the erupting flux rope in the source active region.

This magnetic fieldline stretching model also predicts that there should be a fast-mode wave ahead of the “EIT wave”, which was missed by the EIT telescope because of its low cadence. After the Solar Dynamics Observatory

(SDO) was launched in 2010, its high-cadence observations frequently revealed the co-existence of a fast-moving EUV wave and a slowly-moving EUV wave in an individual event (Chen and Wu, 2011; Asai *et al.*, 2012; Cheng *et al.*, 2012; Shen *et al.*, 2013; White, Balasubramaniam, and Cliver, 2013; Xue *et al.*, 2013; Zong and Dai, 2015). The two wave features are also reproduced in 3D MHD simulations (Downs *et al.*, 2012). According to the magnetic fieldline stretching model (Chen *et al.*, 2002; Chen, Fang, and Shibata, 2005b), the fast-moving EUV waves are the fast-mode wave/shock wave driven by the CME eruption, whereas the slowly-moving EUV waves correspond to the “EIT waves” discovered by Thompson *et al.* (1998). It is noted in passing that Nitta *et al.* (2013) focused on the fastest moving EUV wave and ignored any slowly-moving waves behind in each event of their sample. Therefore, in our understanding, most of the EUV waves in their paper correspond to the fast-mode wave/shock wave, rather than the classical diffuse “EIT waves”.

From the above, it is fair to say that the discovery of the stationary “EIT wave” front in Delannée and Aulanier (1999) and Delannée (2000) played a vital role in challenging the fast-mode wave mode for “EIT waves” and helped colleagues approach a converging viewpoint that there are both wave and non-wave components in EUV wave events (Chen and Fang, 2012; Liu and Ofman, 2014; Warmuth, 2015).

However, recently Chandra *et al.* (2016) analyzed an interesting EUV wave event, where they found that ahead of a slowly-moving “EIT wave” which finally stopped at a magnetic QSL to form a stationary wave front, a fast-moving EUV wave passed through another magnetic QSL, leaving a second stationary front behind. That is to say, a stationary EUV wave can also be formed by the interaction between a fast-mode wave and a magnetic QSL. Such a stationary EUV wave front is different from the stationary “EIT wave” discovered by Delannée and Aulanier (1999) in two aspects. First, in Delannée and Aulanier (1999), the stationary “EIT wave” front is considered as the slowly-moving “EIT wave” asymptotically approaching the magnetic QSL, as simulated by Chen, Fang, and Shibata (2005b, 2006), whereas in Chandra *et al.* (2016), the newly-discovered stationary EUV wave front is formed as a fast-mode wave passes through a magnetic QSL. Second, in Delannée (2000), the stationary “EIT wave” front is copatial with the magnetic QSL, whereas in Chandra *et al.* (2016), the stationary EUV wave front deviates from the magnetic QSL, on the wave-incoming side, as illustrated by Figure 1.

Considering that the magnetic field near a QSL is divergent and the magnetic field (as well as the Alfvén speed) has a local minimum, Chandra *et al.* (2016) tentatively proposed a wave trapping model, *i.e.* as a fast-mode wave propagates across a magnetic QSL which serves as a cavity, part of the fast-mode wave is trapped inside the cavity, being reflected back and forth inside. Regarding the mis-alignment between the stationary wave front and the magnetic QSL, they suggested that it might be due to the low accuracy of the potential field source surface (PFSS) model used to extrapolate the coronal magnetic field.

In this paper, we intend to numerically simulate the interaction of a fast-mode wave with a magnetic QSL. This paper is organized as follows. The numerical method is described in Section 2, and the numerical results are presented in Section 3, which is followed by discussions in Section 4.

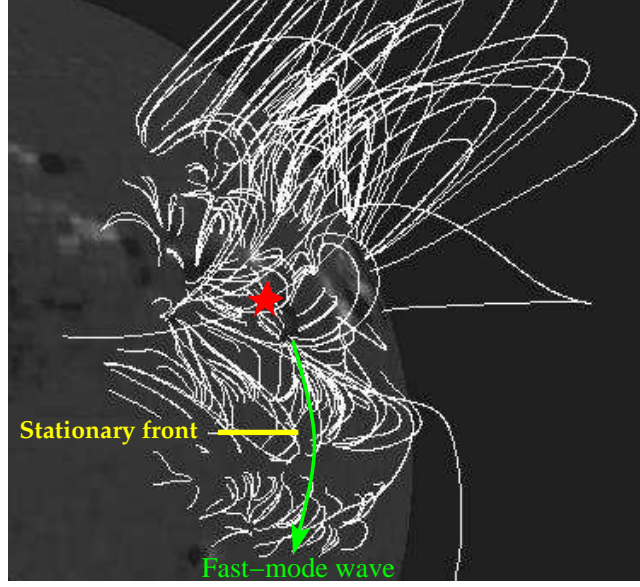


Figure 1. A composite schematic image showing that a fast-mode MHD wave propagates outward (*green line*) from the eruption source region, passing through a magnetic quasi-separatrix layer (QSL) and leaving a stationary front (*yellow line*) to the north of the QSL. The red star marks the eruption source region. The background gray-scale image is the extrapolated potential magnetic field around the CME/flare eruption on 2011 May 11.

2. Numerical Method

For the purpose of this paper, 2-dimensional (2D) ideal MHD equations are sufficient. With the third dimension, z -axis, being ignored, the 2D ideal MHD equations are shown below, which are numerically solved by the multi-step implicit scheme (Hu, 1989; Chen, Fang, and Hu, 2000),

$$\frac{\partial \rho}{\partial t} + \nabla \cdot (\rho \mathbf{v}) = 0, \quad (1)$$

$$\frac{\partial \mathbf{v}}{\partial t} + (\mathbf{v} \cdot \nabla) \mathbf{v} + \frac{1}{\rho} \nabla P - \frac{1}{\rho} \mathbf{j} \times \mathbf{B} + \mathbf{g} = 0, \quad (2)$$

$$\frac{\partial \psi}{\partial t} + \mathbf{v} \cdot \nabla \psi = 0, \quad (3)$$

$$\frac{\partial T}{\partial t} + \mathbf{v} \cdot \nabla T + (\gamma - 1) T \nabla \cdot \mathbf{v} = 0, \quad (4)$$

where the x -axis is horizontal, and the y -axis is vertical, $y = 0$ corresponds to the solar surface, $\gamma = 5/3$ is the ratio of specific heats, \mathbf{g} is the gravity. The five independent variables are density (ρ), velocity (v_x and v_y), magnetic flux

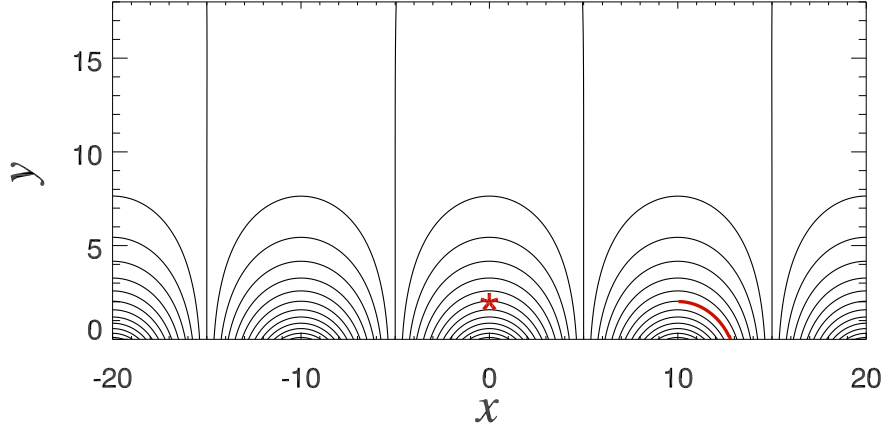


Figure 2. Distribution of the initial magnetic field as shown by the solid lines. The red asterisk marks the location of the pressure-enhanced area, and the red line marks the slice used for the time-distance diagram in Figure 8.

function (ψ), and temperature (T). Here the magnetic field \mathbf{B} is related to the magnetic flux function by $\mathbf{B} = \nabla \times (\psi \hat{\mathbf{e}}_z)$, and $\mathbf{j} = \nabla \times \mathbf{B}$ is the current density. The equations are nondimensionalized with the following characteristic values: $\rho_0 = 1.67 \times 10^{-12} \text{ kg m}^{-3}$, $T_0 = 1 \text{ MK}$, $L_0 = 1.2 \times 10^4 \text{ km}$, $B_0 = 18.6 \text{ G}$. So, the characteristic plasma β is 0.02, the characteristic Alfvén speed is 1286 km s^{-1} , the Alfvén time scale is $\tau_A = 9.33 \text{ s}$.

As shown in Figure 1, the background magnetic field outside the source active region in the observation is characterized by several isolated flux systems divided by magnetic QSLs. In order to mimic such a configuration, we generate a potential magnetic field with periodic QSLs by putting a series of line currents with alternative directions below the solar surface, *i.e.*

$$\psi = \sum_{k=-60}^{k=60} 0.5 \ln[(x+20k)^2 + (y+1.8)^2] - \sum_{k=-60}^{k=59} 0.5 \ln[(x+20k+10)^2 + (y+1.8)^2] \quad (5)$$

in the dimensionless form. The resulting magnetic distribution is displayed in Figure 2, where $x = \pm 5$ and $x = \pm 15$ are the locations of the magnetic QSLs. Note that in 2D, magnetic QSLs degenerate into separatrices (Démoulin, 2006).

The initial temperature is set to be uniform with the normalized $T = 1$ everywhere. The initial atmosphere is in hydrostatic equilibrium, *i.e.* the density decays exponentially with height in the dimensionless form $\rho = \exp(-\gamma gy)$. The dimensionless size of the simulation domain is $-20 \leq x \leq 20$ and $0 \leq y \leq 18$. Calculation is performed in the right half zone because of symmetry. The calculation area is discretized by 138×541 grid points, which are uniformly distributed in the y -direction and nonuniformly distributed in the x -direction, with grid points slightly more concentrated near the y -axis. Symmetry conditions are specified along the left boundary ($x = 0$), whereas the top ($y = 18$) and the right-hand ($x = 20$) sides are treated as open boundaries, which allow plasmas

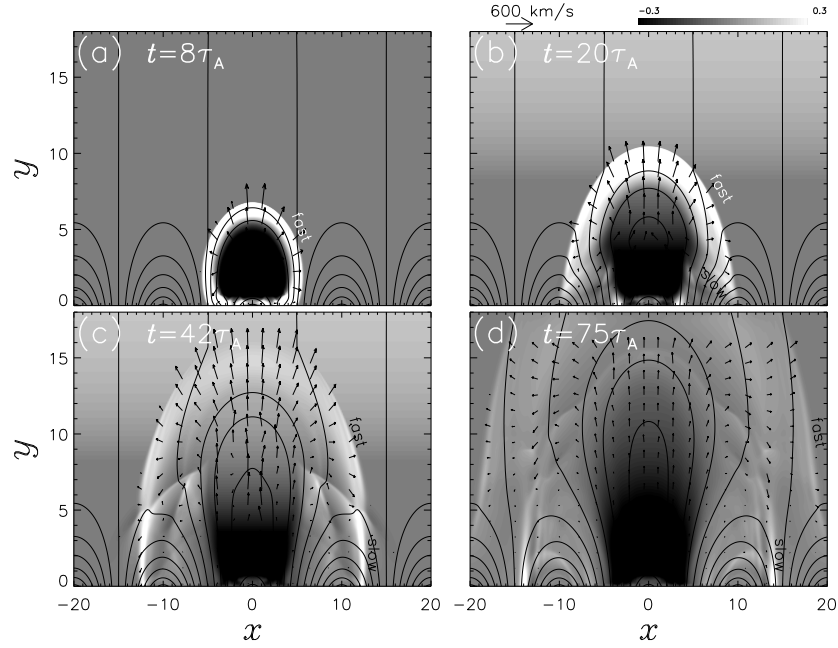


Figure 3. Evolution of the density variation (*gray scale*), magnetic field (*solid lines*), and velocity (*arrows*). Note that the dimensionless density enhancement near the shock wave front can be much larger than 0.3. The scale bar is truncated at 0.3 in order to highlight the weak variation.

to move out or come in. Besides, line-tying effect is considered on the bottom boundary, *i.e.* the values of the velocity ($v_x = v_y = 0$) and ψ are fixed. Besides, the density is also fixed, whereas the temperature gradient is set to be zero.

Strictly speaking, the fast-mode coronal shock waves, especially those that can generate chromospheric Moreton waves, are generally thought to be driven by erupting CMEs, or erupting flux ropes in a strict sense, rather than by the pressure pulse inside solar flares (Cliver, Webb, and Howard, 1999; Chen *et al.*, 2002). However, in this paper, we are not interested in the driving mechanism of the shock wave, therefore we use the simplest way to drive a fast-mode shock wave, *i.e.* by putting an artificially high gas pressure inside a small circular area $x^2 + (y - 2)^2 \leq 0.5^2$, as indicated by the asterisk in Figure 2. Inside this area, the locally enhanced temperature is distributed as $T = 2001 - 2000[x^2 + (y - 2)^2]/0.5^2$, which decreases from 2001 at the center to 1 at the boundary of this circular area.

3. Numerical Results

The high gas pressure around the position ($x = 0$, $y = 2$) initiates a circular shock wave propagating outward, as shown by the outermost wave front which is marked by “fast” in Figure 3. This figure displays the evolution of the base difference of the density distribution (*gray-scale*), magnetic field (*solid lines*),

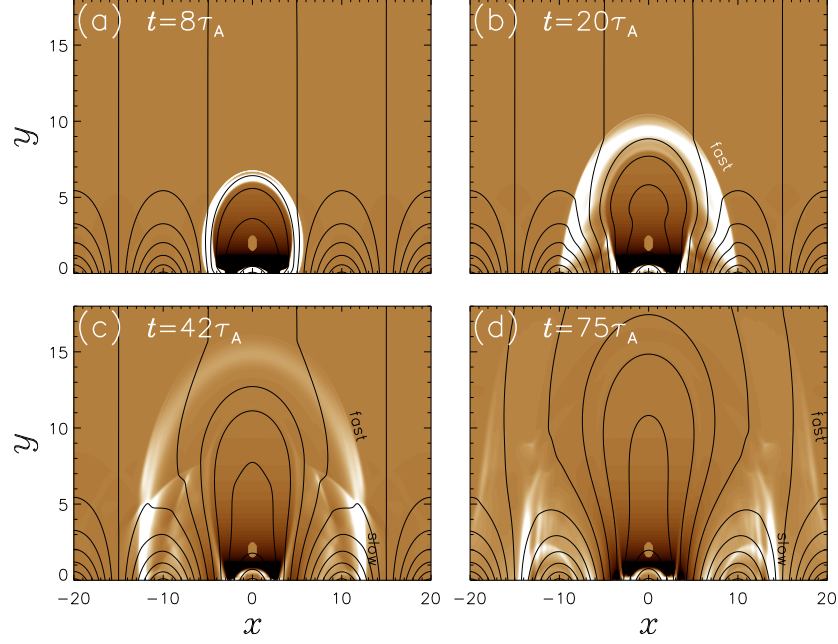


Figure 4. Evolution of the base-difference EUV 193 Å distribution (*color scale*), magnetic field (*solid lines*), and velocity (*arrows*), where the EUV 193 Å distribution is synthesized from the simulation results.

and velocity (*arrows*). As the shock wave expands, it becomes very similar to the piston-driven shock wave straddling over the source active region as numerically simulated by Chen *et al.* (2002). The two flanks of the shock wave sweep the flux systems in the background and the separatrices between neighboring flux systems. As revealed by Figure 3, the shock passes through the first separatrix at $x = 5$ (and its symmetric one on the negative x -axis) around $t = 8\tau_A$, leaving nearly nothing behind. At $t = 20\tau_A$, the footpoint of the shock wave approaches the core of the neighboring flux system. Since the magnetic field is stronger toward the core, the leg part of the shock front is refracted upward slightly. At the same time, another bright front, to the right of the label “slow”, appears behind the shock wave, which intersects with the shock wave at $(x = 9.2, y = 1.4)$. At $t = 42\tau_A$ as shown by Figure 3c, the bright patch, which is at around $x = 12$ as marked by “slow”, becomes vertical, and actually decouples from the outermost shock wave. Thereafter, the outermost fast-mode shock wave keeps expanding rapidly, whereas the bright vertical patch moves outward extremely slowly. At $t = 75\tau_A$ as shown by Figure 3d, the footpoint of the outermost shock wave reaches the right boundary at $x = 20$. However, the bright patch is still at around $x = 14$, as marked by the label “slow”. Finally, the bright patch is seen to stop near $x = 14$, never reaching the location of the magnetic separatrix at $x = 15$.

In order to compare the numerical results with the SDO/AIA observations, we synthesize the AIA 193 Å intensity map based on the plasma density, temper-

ature, and the AIA response function. The AIA 193 Å emission of the numerical results in Figure 3 is presented in Figure 4, which shows the evolution of the AIA 193 Å base-difference map (*color*) and the magnetic field (*solid lines*). Note that the base-difference map is derived by subtracting the initial intensity from each time step. The evolution of the 193 Å map is very similar to that of the density map, which is due to the fact that the EUV emission is proportional to the density squared.

Suppose that the whole evolution presented in Figure 4 is observed from above, we can obtain the time-distance diagram of the wave propagation. Figure 5 depicts the time evolution of the AIA 193 Å intensity distribution along the positive x -axis. Note that the AIA 193 Å intensity distribution is derived by integrating the 2D images in Figure 4 over the y -direction. It is seen from Figure 5 that the fast-mode shock wave, as indicated by the white arrow, propagates outward with an initial velocity of 510 km s^{-1} . At around $t = 40\tau_A$, the shock wave front bifurcates into two branches: A brighter one slows down rapidly, and finally approaches but never reaches the separatrix at $x = 15$ (hence we call it quasi-stationary wave front); The other weaker wave with a dimming edge (**near the white thick arrow**) follows the original trajectory, and keeps propagating outward. The dimming edge has a velocity slightly smaller than 510 km s^{-1} , but the emissive front has a velocity of only 260 km s^{-1} .

Figure 5 also reveals several other wave patterns. One bright wave appears at the distance of 5 at $t = 27\tau_A$. This wave, which is one of the wave train driven by the locally enhanced gas pressure, has the same fate as the primary shock wave, *e.g.* it bifurcates into a brighter quasi-stationary wave and a weaker fast-moving wave at $t = 77\tau_A$. There is also a trapped wave, bouncing back and forth between $x = 0$ and $x = 2$, which results from the slow-mode wave propagating along the magnetic loop threading the gas pressure enhanced area around $(x = 0, y = 2)$. The formation of these waves is related to the *ad hoc* generation method of the primary shock wave adopted in this paper. In real observations, they are not necessarily present.

4. Discussions

“EIT waves” were discovered more than 18 years ago with the SOHO/EIT telescope (Thompson *et al.*, 1998). The poor cadence of the telescope, as well as the relatively lower spatial resolution, incurred many controversies, including the driving source and the nature of this spectacular phenomenon (for reviews, see Wills-Davey and Attrill, 2009; Gallagher and Long, 2011; Chen and Fang, 2012; Patsourakos and Vourlidas, 2012; Liu and Ofman, 2014; Warmuth, 2015; Chen, 2016). Initially it was widely thought that “EIT waves” are fast-mode waves. However, the discovery of a stationary “EIT wave” front, as well as the significantly lower velocities of “EIT waves” compared to type II radio bursts or Moreton waves, invoked several groups to propose non-wave models, such as the magnetic fieldline stretching model (Chen *et al.*, 2002; Chen, Ding, and Fang, 2005a; Chen, Fang, and Shibata, 2005b; Yang and Chen, 2010; Chen, 2009), the slow-mode wave model (Wills-Davey, DeForest, and Stenflo, 2007; Wang, Shen,

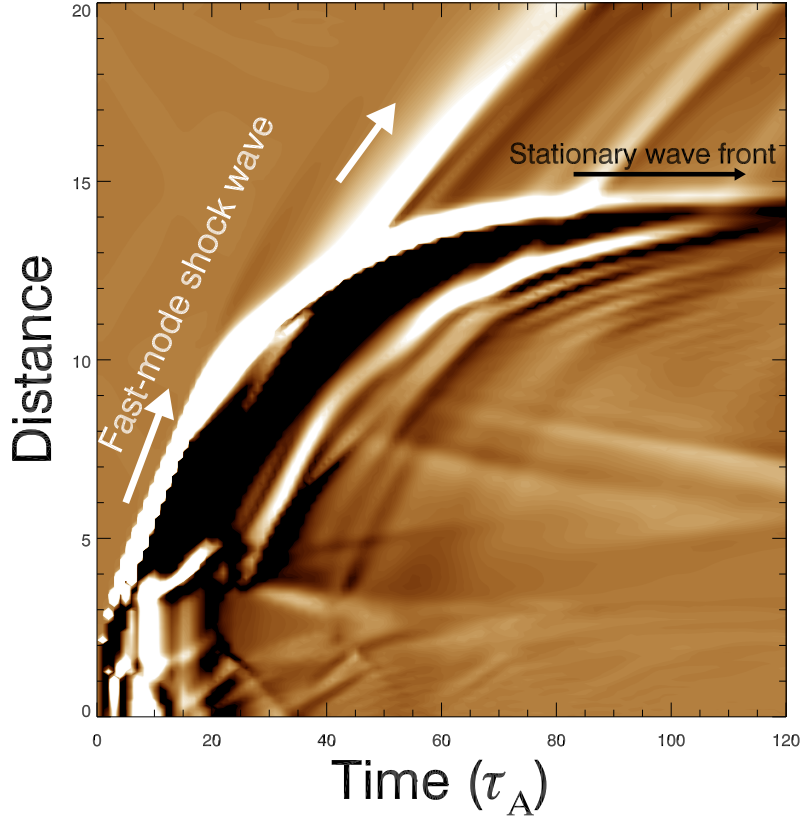


Figure 5. Time evolution of the 193 Å difference intensity distribution along positive x -axis when the numerical results in Figure 4 are viewed from above. The start point of the distance is at $x = 0$. The shock wave travels with an initial velocity of 510 km s^{-1} , which decelerates to 260 km s^{-1} after $t \sim 40\tau_A$. A quasi-stationary wave front emanates from the fast-mode wave, and approaches the distance around $x = 14$.

and Lin, 2009; Mei, Udo, and Lin, 2012), the successive reconnection model (Attrill *et al.*, 2007a), and the current shell model (Delannée *et al.*, 2008).

When putting forward the magnetic fieldline stretching model for “EIT waves”, Chen *et al.* (2002) and Chen, Fang, and Shibata (2005b) predicted that there should be two types of waves co-existing in EUV images if only the observational cadence is high enough, *i.e.* there are in principle two EUV waves in one event, with the faster one being a fast-mode MHD wave and the slower one being the “EIT waves” due to the successive stretching of the closed magnetic field lines pushed by an erupting flux rope.

After the launch of the SDO satellite in 2010, its onboard AIA telescope routinely provides EUV images with unprecedentedly high spatiotemporal resolutions. On the one hand, various groups reported the co-existence of two EUV waves in many individual events (Harra and Sterling, 2003; Chen and Wu, 2011; Asai *et al.*, 2012; Cheng *et al.*, 2012; Zheng *et al.*, 2012; Shen *et al.*, 2013; White, Balasubramaniam, and Cliver, 2013; Xue *et al.*, 2013). On the other

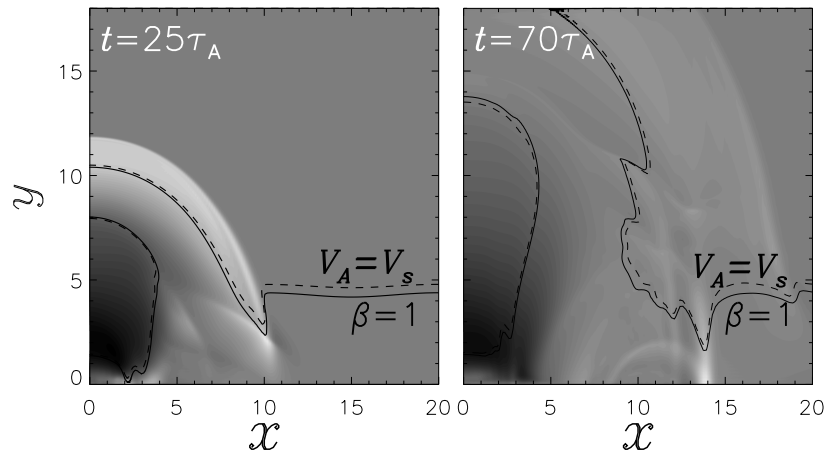


Figure 6. Evolution of the density variation (gray scale) and the contour lines with the plasma $\beta = 1$ and $\beta = 2/\gamma$ (*i.e.* the Alfvén speed V_A equals the sound speed V_s).

hand, SDO/AIA revealed several features that were not seen before. For example, Guo, Ding, and Chen (2015) found that behind the fast-mode wave (or shock wave), there is not a continual slower “EIT wave”. Instead, there are two or three patchy wave fronts with extremely low speeds such as 30 km s^{-1} for each, which are more than 20 times smaller than the speed of the fast-mode wave. However, if connected together, these patchy wave fronts form a pattern which is very similar to the classical “EIT waves”, with an apparent speed of ~ 3 times smaller than that of the corresponding fast-mode wave in the same event. They illustrated how this feature can be explained by the magnetic fieldline stretching model proposed by Chen *et al.* (2002).

Another new and unexpected feature was recently found by Chandra *et al.* (2016). In their event, besides the co-existing fast-mode wave and slower “EIT wave” (the latter of which finally stops at a magnetic QSL), the fast-mode wave passes through another magnetic QSL, leaving a stationary EUV wave front behind. In order to understand the formation mechanism of this stationary EUV wave front, we numerically simulated the passage of a fast-mode shock wave through a magnetic QSL. It is found that as the shock wave sweeps the isolated flux system, a newly-formed bright front emanates from the leg part of the fast-mode shock wave, as indicated by Figure 3. This bright front is in the wake of the fast-mode shock wave, and moves extremely slowly before finally stopping at $x = 14$, which is not cospatial but very close to the neighboring separatrix at $x = 15$. Such a quasi-stationary wave front is very similar to the observations analyzed by Chandra *et al.* (2016), *i.e.* when a fast-mode wave runs through an isolated flux system, a quasi-stationary EUV wave front is left while the fast-mode wave keeps moving outward. More interestingly, our simulation results indicate that the stationary front is offset from the nearby magnetic separatrix, which is exactly what was observed by Chandra *et al.* (2016).

It has been well established that as a fast-mode wave penetrates into the site with weak magnetic field where the Alfvén speed is comparable with the

sound speed, part of the fast-mode wave would be converted to a slow-mode wave (Cally, 2005). Such a situation can happen in the case of weak magnetic field, *e.g.* in the corona near magnetic null points (McLaughlin and Hood, 2006). It can also happen in the terrestrial magnetosphere (Nakariakov *et al.*, 2016). In the case of an isolated magnetic flux system which is bordered by magnetic QSLs, the coronal magnetic field above the flux system can be very weak since the magnetic field over the QSLs are strongly divergent. Hence, it is expected that at a certain height, the coronal Alfvén speed (v_A) is comparable with the sound speed (v_s), and the mode conversion can happen here. In order to confirm this, we plot the contour lines with $\beta = 1$ (*solid line*) and $\beta = 2/\gamma$ (*dashed line*) over the distribution of the density (*gray scale*) in Figure 6. Note that the plasma $\beta = 2/\gamma$ corresponds to $v_A = v_s$. It is seen that around $t = 25\tau_A$ the leg of the primary shock wave begins to bifurcate near the location with $\beta = 1$. Whereas the ongoing fast-mode wave becomes fainter, the slower wave becomes remarkably bright, and moves slowly. We conjecture that this slowly-moving bright front is a slow-mode MHD wave converted from the primary fast-mode wave.

In order to confirm the slow-mode wave nature of this bright front, we compare the distributions of v_{\parallel} and v_{\perp} of the numerical results in Figure 7, where v_{\parallel} is the component of the plasma velocity parallel to the local magnetic field, whereas v_{\perp} is the component of the plasma velocity perpendicular to the local magnetic field. As demonstrated by Bogdan *et al.* (2003), the v_{\parallel} map highlights the slow-mode waves, whereas the v_{\perp} map highlights the fast-mode waves. From Figure 7, it is seen that the quasi-stationary bright wave front is indeed a slow-mode wave. It is noticed that the upper part of the primary fast-mode shock wave is also bright in the v_{\parallel} map since the upper corona is high- β plasma, and the fast-mode wave front there has acoustic nature.

The location of the bright slow-mode wave apparently moves slowly from $x = 13$ at $t = 42\tau_A$ to $x = 14$ at $t = 75\tau_A$ as seen from Figure 4. By examining the movie of the evolution, it is found that each segment of the wave front is actually propagating along the magnetic field line. In order to derive the field-aligned propagation velocity, we select a curved slice along the magnetic field line, which is marked in Figure 2 as the thick red arc. The time-distance diagram of the density distribution is displayed in Figure 8. It is seen that the bright front travels along the closed magnetic field line with a speed of 186 km s^{-1} , which is exactly the sound speed in the simulation where the plasma temperature is $\sim 1.2 \text{ MK}$. This further confirms that the quasi-stationary bright front is a slow-mode wave converted from the passing fast-mode shock wave.

Having said so, another question arises: As shown by Figure 6, the $v_A = v_s$ line covers the whole layer from left to right, so why the mode conversion becomes evident only when the passing fast-mode wave arrives at $x = 11$? We suggest that this is probably related to the efficiency of the mode conversion. According to Cally (2005), the fast-to-slow mode conversion is the most efficient when the wave vector is parallel to the local magnetic field. As discerned from Figure 3, the mode conversion indeed happens when the incoming wave front is nearly perpendicular to the magnetic field lines, *i.e.* the wave vector is parallel to the field lines. That is to say, two factors lead to the wave mode conversion at

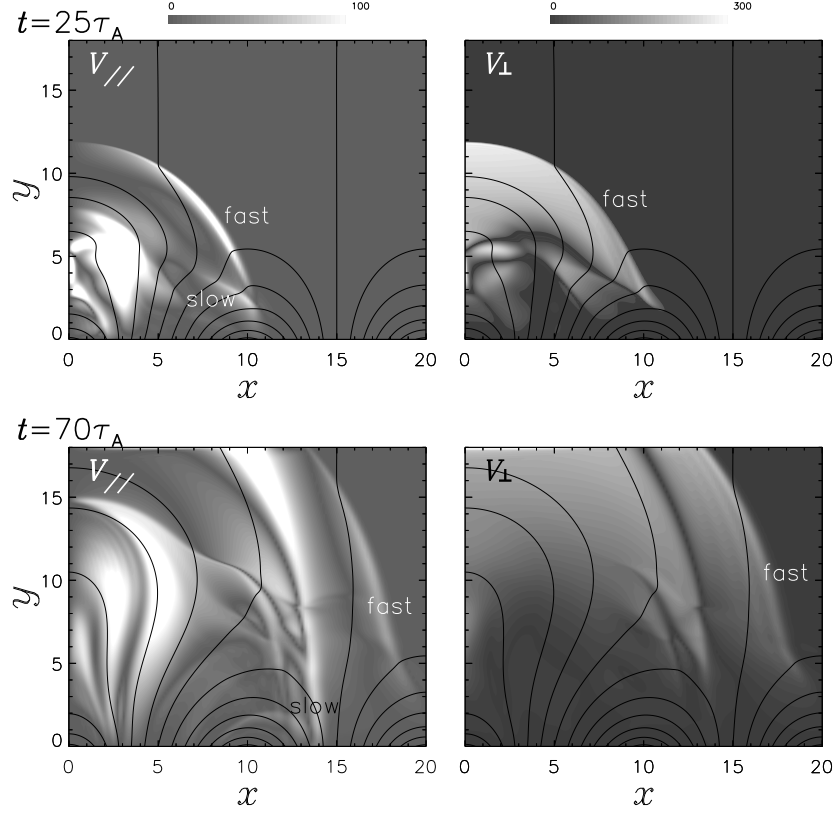


Figure 7. Top: Distributions of v_{\parallel} and v_{\perp} (gray scale) at $t = 25\tau_A$, where the magnetic field (solid lines) is superposed; Bottom: Distributions of v_{\parallel} and v_{\perp} (gray scale) at $t = 70\tau_A$, where the magnetic field (solid lines) is superposed.

$x = 11$: the divergent flux tubes near the magnetic separatrix result in a region with $\beta \sim 1$; meanwhile the magnetic field is roughly parallel to the shock wave normal here.

To summarize, with MHD numerical simulations, we investigated the interaction between an incoming fast-mode shock wave and an isolated magnetic flux system bordered by magnetic separatrices. It is revealed that when the fast-mode shock wave penetrates into the flux system, part of the fast-mode wave is converted to a slow-mode wave, which then travels along the magnetic field lines with the local sound speed. Apparently the location of the wave front is shifted across the magnetic field lines slightly, and sweeps the solar surface with a smaller and smaller velocity. Finally, the slow-mode wave stops at the location in front of the magnetic separatrix. The final location where the quasi-stationary front stops depends on the highest magnetic loop where the mode conversion occurs, since the converted slow-mode wave segment travels along the magnetic loop. This implies that a stationary EUV wave front, which was originally used as one the main reasons to challenge the fast-mode wave model for “EIT waves”

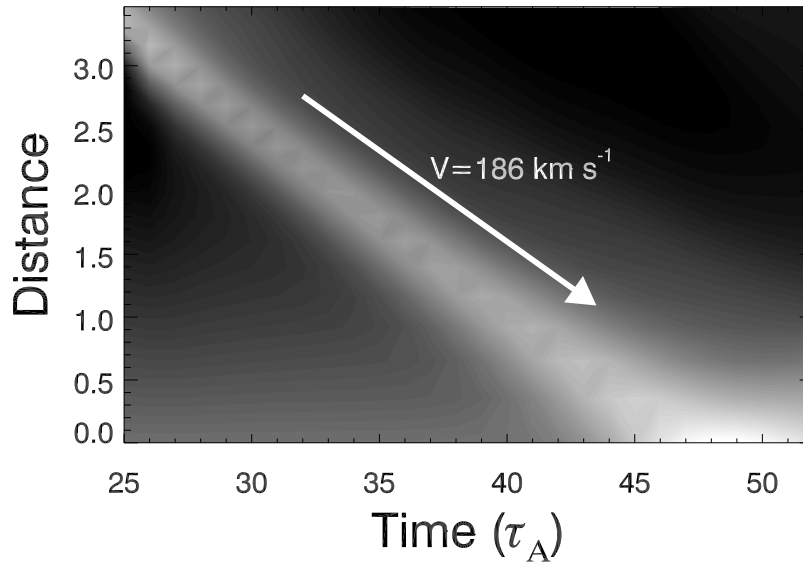


Figure 8. Time-distance diagram of the density distribution along the slice with $\psi = 7.7$ between $x = 10$ and $x = 12.7$. The slice is marked as the red arc in Figure 2. The white ridge corresponds to the converted wave travelling along the same magnetic field line with a propagation velocity of 186 km s^{-1} .

(Delannée and Aulanier, 1999; Chen, Fang, and Shibata, 2005b), can also be produced by fast-mode waves via the mode conversion at the layer where the Alfvén speed is comparable to the sound speed. The slow-mode wave, trapped inside the magnetic loop, travels along the magnetic field line to the footpoint of the field line, forming a quasi-stationary wave front. However, it should be pointed again that such a stationary wave front is different from the stationary “EIT waves” in two aspects: (1) In the former case, the incident fast-mode wave keeps going, leaving a stationary wave front behind. However, in the latter case, the slowly-moving “EIT wave” gradually decelerates to form a stationary front; (2) The stationary wave front generated by the mode conversion from a passing fast-mode wave is offset from the magnetic QSL, whereas the stationary “EIT wave” is generally cospatial with the magnetic QSL, as demonstrated by Delannée (2000) and Chen, Fang, and Shibata (2005b, 2006). Future spectroscopic observations as in Madjarska, Doyle, and Shetye (2015) and Vanninathan *et al.* (2015) might dig out more differences between these two types of stationary fronts.

It is noted in passing that fast-mode MHD waves are frequently generated by the CME/flare eruptions (Aschwanden *et al.*, 1999; Nakariakov *et al.*, 1999; Liu *et al.*, 2011; Su *et al.*, 2015; Vršnak *et al.*, 2016), and magnetic QSLs are also distributed all over the solar surface, therefore, the mode conversion studied in this paper might happen frequently, which deserves further studies.

Acknowledgments The authors are grateful to the referee for the constructive suggestions. This research was supported by the Chinese foundations NSFC (11533005 and 11025314),

2011CB811402, and Jiangsu 333 Project. PFC thanks the ISSI-Beijing office for organizing a wave workshop, where the discussions inspired the ideas presented in this paper.

References

- Asai, A., Ishii, T.T., Isobe, H., Kitai, R., Ichimoto, K., UeNo, S., Nagata, S., Morita, S., Nishida, K., Shiota, D., Oi, A., Akioka, M., Shibata, K.: 2012, *Astrophys. J. Lett.* **745**, L18. doi:10.1088/2041-8205/745/2/L18.
- Aschwanden, M.J., Fletcher, L., Schrijver, C.J., Alexander, D.: 1999, *Astrophys. J.* **520**, 880. doi:10.1086/307502.
- Attrill, G.D.R., Harra, L.K., van Driel-Gesztelyi, L., Démoulin, P., Wülser, J.P.: 2007, *Astronomische Nachrichten* **328**, 760. doi:10.1002/asna.200710794.
- Attrill, G.D.R., Harra, L.K., van Driel-Gesztelyi, L., Démoulin, P.: 2007, *Astrophys. J. Lett.* **656**, L101. doi:10.1086/512854.
- Biesecker, D.A., Myers, D.C., Thompson, B.J., Hammer, D.M., Vourlidas, A.: 2002, *Astrophys. J.* **569**, 1009. doi:10.1086/339402.
- Bogdan, T.J., Carlsson, M., Hansteen, V.H., *et al.*: 2003, *Astrophys. J.* **599**, 626. doi:10.1086/378512.
- Cally, P.S.: 2005, *Mon. Not. Roy. Astron. Soc.* **358**, 353. doi:10.1111/j.1365-2966.2005.08742.x.
- Chandra, R., Chen, P.F., Fulara, A., Srivastava, A.K., Uddin, W.: 2016, *Astrophys. J.* **in press**. doi:to be assigned.
- Chen, P., Fang, C., Hu, Y.: 2000, *Chinese Science Bulletin* **45**, 798.
- Chen, P.F.: 2006, *Astrophys. J. Lett.* **641**, L153. doi:10.1086/503868.
- Chen, P.F.: 2009, *Science in China: Physics, Mechanics and Astronomy* **52**, 1785. doi:10.1007/s11433-009-0240-9.
- Chen, P.F.: 2011, *Living Reviews in Solar Physics* **8**, 1. doi:10.12942/lrsp-2011-1.
- Chen, P.F.: 2016, *Low-frequency waves in space plasmas*, First edition edn., *Geophysical Monograph* **216**, John Wiley & Sons, Inc., USA, 381.
- Chen, P.F., Fang, C.: 2012, In: Faurobert, M., Fang, C., Corbard, T. (eds.) *EAS Publications Series*, *EAS Publications Series* **55**, 313. doi:10.1051/eas/1255043.
- Chen, P.F., Wu, Y.: 2011, *Astrophys. J. Lett.* **732**, L20. doi:10.1088/2041-8205/732/2/L20.
- Chen, P.F., Ding, M.D., Fang, C.: 2005, *Space Sci. Rev.* **121**, 201. doi:10.1007/s11214-006-3911-0.
- Chen, P.F., Fang, C., Shibata, K.: 2005, *Astrophys. J.* **622**, 1202. doi:10.1086/428084.
- Chen, P.F., Fang, C., Shibata, K.: 2006, *Advances in Space Research* **38**, 456. doi:10.1016/j.asr.2005.01.049.
- Chen, P.F., Wu, S.T., Shibata, K., Fang, C.: 2002, *Astrophys. J. Lett.* **572**, L99. doi:10.1086/341486.
- Cheng, X., Zhang, J., Olmedo, O., Vourlidas, A., Ding, M.D., Liu, Y.: 2012, *Astrophys. J. Lett.* **745**, L5. doi:10.1088/2041-8205/745/1/L5.
- Cliwer, E.W., Webb, D.F., Howard, R.A.: 1999, *Solar Phys.* **187**, 89. doi:10.1023/A:1005115119661.
- Cohen, O., Attrill, G.D.R., Manchester, W.B. IV, Wills-Davey, M.J.: 2009, *Astrophys. J.* **705**, 587. doi:10.1088/0004-637X/705/1/587.
- Cohen, O., Attrill, G.D.R., Schwadron, N.A., Crooker, N.U., Owens, M.J., Downs, C., Gombosi, T.I.: 2010, *Journal of Geophysical Research (Space Physics)* **115**, A10104. doi:10.1029/2010JA015464.
- Delaboudinière, J.P., Artzner, G.E., Brunaud, J., *et al.*: 1995, *Solar Phys.* **162**, 291. doi:10.1007/BF00733432.
- Delannée, C.: 2000, *Astrophys. J.* **545**, 512. doi:10.1086/317777.
- Delannée, C., Aulanier, G.: 1999, *Solar Phys.* **190**, 107. doi:10.1023/A:1005249416605.
- Delannée, C., Török, T., Aulanier, G., Hochedez, J.F.: 2008, *Solar Phys.* **247**, 123. doi:10.1007/s11207-007-9085-4.
- Démoulin, P.: 2006, *Advances in Space Research* **37**, 1269. doi:10.1016/j.asr.2005.03.085.
- Downs, C., Roussev, I.I., van der Holst, B., Lugaz, N., Sokolov, I.V.: 2012, *Astrophys. J.* **750**, 134. doi:10.1088/0004-637X/750/2/134.
- Gallagher, P.T., Long, D.M.: 2011, *Space Sci. Rev.* **158**, 365. doi:10.1007/s11214-010-9710-7.

- Grechnev, V.V., Uralov, A.M., Chertok, I.M., Slemzin, V.A., Filippov, B.P., Egorov, Y.I., Fainshtein, V.G., Afanasyev, A.N., Prestage, N.P., Temmer, M.: 2014, *Solar Phys.* **289**, 1279. doi:10.1007/s11207-013-0397-2.
- Grechnev, V.V., Uralov, A.M., Kuzmenko, I.V., Kochanov, A.A., Chertok, I.M., Kalashnikov, S.S.: 2015, *Solar Phys.* **290**, 129. doi:10.1007/s11207-014-0621-8.
- Guo, Y., Ding, M.D., Chen, P.F.: 2015, *Astrophys. J. Suppl.* **219**, 36. doi:10.1088/0067-0049/219/2/36.
- Harra, L.K., Sterling, A.C.: 2003, *Astrophys. J.* **587**, 429. doi:10.1086/368079.
- Hu, Y.Q.: 1989, *Journal of Computational Physics* **84**(2), 441. doi:10.1016/0021-9991(89)90242-8.
- Klassen, A., Aurass, H., Mann, G., Thompson, B.J.: 2000, *Astron. Astrophys. Suppl.* **141**, 357. doi:10.1051/aas:2000125.
- Kumar, P., Cho, K.S., Chen, P.F., Bong, S.C., Park, S.H.: 2013, *Solar Phys.* **282**, 523. doi:10.1007/s11207-012-0158-7.
- Liu, W., Ofman, L.: 2014, *Solar Phys.* **289**, 3233. doi:10.1007/s11207-014-0528-4.
- Liu, W., Title, A.M., Zhao, J., Ofman, L., Schrijver, C.J., Aschwanden, M.J., De Pontieu, B., Tarbell, T.D.: 2011, *Astrophys. J. Lett.* **736**, L13. doi:10.1088/2041-8205/736/1/L13.
- Long, D.M., Gallagher, P.T., McAteer, R.T.J., Bloomfield, D.S.: 2008, *Astrophys. J. Lett.* **680**, L81. doi:10.1086/589742.
- Madjarska, M.S., Doyle, J.G., Shetye, J.: 2015, *Astron. Astrophys.* **575**, A39. doi:10.1051/0004-6361/201424754.
- McLaughlin, J.A., Hood, A.W.: 2006, *Astron. Astrophys.* **459**, 641. doi:10.1051/0004-6361:20065558.
- Mei, Z., Udo, Z., Lin, J.: 2012, *Science China Physics, Mechanics, and Astronomy* **55**, 1316. doi:10.1007/s11433-012-4752-3.
- Moses, D., Clette, F., Delaboudinière, J.P., et al.: 1997, *Solar Phys.* **175**, 571. doi:10.1023/A:1004902913117.
- Nakariakov, V.M., Ofman, L., Deluca, E.E., Roberts, B., Davila, J.M.: 1999, *Science* **285**, 862. doi:10.1126/science.285.5429.862.
- Nakariakov, V.M., Pilipenko, V., Heilig, B., Jelínek, P., Karlický, M., Klimushkin, D.Y., Kolotkov, D.Y., Lee, D.H., Nisticò, G., Van Doorselaere, T., Verth, G., Zimovets, I.V.: 2016, *Space Sci. Rev.* doi:10.1007/s11214-015-0233-0.
- Nitta, N.V., Schrijver, C.J., Title, A.M., Liu, W.: 2013, *Astrophys. J.* **776**, 58. doi:10.1088/0004-637X/776/1/58.
- Ofman, L., Thompson, B.J.: 2002, *Astrophys. J.* **574**, 440. doi:10.1086/340924.
- Patsourakos, S., Vourlidas, A.: 2012, *Solar Phys.* **281**, 187. doi:10.1007/s11207-012-9988-6.
- Shen, Y., Liu, Y., Su, J., Li, H., Zhao, R., Tian, Z., Ichimoto, K., Shibata, K.: 2013, *Astrophys. J. Lett.* **773**, L33. doi:10.1088/2041-8205/773/2/L33.
- Su, W., Cheng, X., Ding, M.D., Chen, P.F., Sun, J.Q.: 2015, *Astrophys. J.* **804**, 88. doi:10.1088/0004-637X/804/2/88.
- Thompson, B.J., Plunkett, S.P., Gurman, J.B., Newmark, J.S., St. Cyr, O.C., Michels, D.J.: 1998, *Geophys. Res. Lett.* **25**, 2465. doi:10.1029/98GL50429.
- Thompson, B.J., Gurman, J.B., Neupert, W.M., Newmark, J.S., Delaboudinière, J.P., Cyr, O.C.S., Stezelberger, S., Dere, K.P., Howard, R.A., Michels, D.J.: 1999, *Astrophys. J. Lett.* **517**, L151. doi:10.1086/312030.
- van Driel-Gesztelyi, L., Attrill, G.D.R., Démoulin, P., Mandrini, C.H., Harra, L.K.: 2008, *Annales Geophysicae* **26**, 3077. doi:10.5194/angeo-26-3077-2008.
- Vanninathan, K., Veronig, A.M., Dissauer, K., Madjarska, M.S., Hannah, I.G., Kontar, E.P.: 2015, *Astrophys. J.* **812**, 173. doi:10.1088/0004-637X/812/2/173.
- Veronig, A.M., Temmer, M., Vršnak, B.: 2008, *Astrophys. J. Lett.* **681**, L113. doi:10.1086/590493.
- Vršnak, B., Warmuth, A., Brajša, R., Hanslmeier, A.: 2002, *Astron. Astrophys.* **394**, 299. doi:10.1051/0004-6361:20021121.
- Vršnak, B., Žic, T., Lulić, S., Temmer, M., Veronig, A.M.: 2016, *Solar Phys.* **291**, 89. doi:10.1007/s11207-015-0822-9.
- Wang, H., Shen, C., Lin, J.: 2009, *Astrophys. J.* **700**, 1716. doi:10.1088/0004-637X/700/2/1716.
- Wang, Y.M.: 2000, *Astrophys. J. Lett.* **543**, L89. doi:10.1086/318178.
- Warmuth, A.: 2015, *Living Reviews in Solar Physics* **12**. doi:10.1007/lrsp-2015-3.
- White, S.M., Balasubramaniam, K., Cliver, E.: 2013, *Technical report of Air Force Research Laboratory* **22**, 1.

-
- Wills-Davey, M.J., Attrill, G.D.R.: 2009, *Space Sci. Rev.* **149**, 325. doi:10.1007/s11214-009-9612-8.
- Wills-Davey, M.J., Thompson, B.J.: 1999, *Solar Phys.* **190**, 467. doi:10.1023/A:1005201500675.
- Wills-Davey, M.J., DeForest, C.E., Stenflo, J.O.: 2007, *Astrophys. J.* **664**, 556. doi:10.1086/519013.
- Wu, S.T., Zheng, H., Wang, S., Thompson, B.J., Plunkett, S.P., Zhao, X.P., Dryer, M.: 2001, *J. Geophys. Res.* **106**, 25089. doi:10.1029/2000JA000447.
- Xue, Z.K., Qu, Z.Q., Yan, X.L., Zhao, L., Ma, L.: 2013, *Astron. Astrophys.* **556**, A152. doi:10.1051/0004-6361/201220731.
- Yang, H.Q., Chen, P.F.: 2010, *Solar Phys.* **266**, 59. doi:10.1007/s11207-010-9595-3.
- Zhang, Y., Kitai, R., Narukage, N., Matsumoto, T., Ueno, S., Shibata, K., Wang, J.: 2011, *Pub. Astron. Soc. Japan* **63**, 685. doi:10.1093/pasj/63.3.685.
- Zheng, R., Jiang, Y., Yang, J., Bi, Y., Hong, J., Yang, B., Yang, D.: 2012, *Astrophys. J.* **747**, 67. doi:10.1088/0004-637X/747/1/67.
- Zhukov, A.N., Auchère, F.: 2004, *Astron. Astrophys.* **427**, 705. doi:10.1051/0004-6361:20040351.
- Zong, W., Dai, Y.: 2015, *Astrophys. J.* **809**, 151. doi:10.1088/0004-637X/809/2/151.